Full title:

Interactive effect of beta-adrenergic stimulation and mechanical stretch on low-frequency oscillations of ventricular action potential duration in humans

Authors:

Esther Pueyo PhD[a,b], Michele Orini PhD[c], José F. Rodríguez PhD[d], Peter Taggart MD DSc[c]

Institutions:

[a]Biomedical Signal Interpretation and Computational Simulation (BSICoS) group, Aragón Institute of Engineering Research, IIS Aragón, University of Zaragoza. Edificio I+D+I, C/ Mariano Esquillor s/n. 50018, Zaragoza, Spain.

[b]Biomedical Research Networking Center in Bioengineering, Biomaterials and Nanomedicine (CIBER-BBN), Instituto de Salud Carlos III. C/ Monforte de Lemos 3-5, pabellón 11, planta 0. 28029, Madrid, Spain.

[c]Institute of Cardiovascular Science, University College London. Gower Street. WC1E 6BT, London, United Kingdom.

[d]LaBS, Department of Chemistry, Materials and Chemical Engineering 'Giulio Nata', Politecnico di Milano. Piazza Leonardo da Vinci, 32. 20133, Milano, Italy.

Corresponding author and address

Dr Esther Pueyo,

BSICoS group, I3A, University of Zaragoza

Edificio I+D+I, C/ Mariano Esquillor s/n.

50018 Zaragoza, Spain

E-mail: epueyo@unizar.es

Abstract

Ventricular repolarization dynamics are crucial to arrhythmogenesis. Low-frequency oscillations of repolarization have recently been reported in humans and the magnitude of these oscillations shown to be a strong predictor of sudden cardiac death. Available evidence suggests a role of the sympathetic nervous system. We have used biophysically detailed models integrating ventricular electrophysiology, calcium dynamics, mechanics and β-adrenergic signaling to investigate the underlying mechanisms. The main results were: (1) Phasic beta-adrenergic stimulation (β-AS) at a Mayer wave frequency between 0.03 and 0.15 Hz resulted in a gradual decrease of action potential (AP) duration (APD) with concomitant small APD oscillations. (2) After 3-4 minutes of phasic β-AS, the mean APD adapted and oscillations of APD became apparent. (3) Phasic changes in haemodynamic loading at the same Mayer wave frequency (a known accompaniment of enhanced

sympathetic nerve activity), simulated as variations in the sarcomere length, also induced APD oscillations. (4) The effect of phasic β-AS and haemodynamic loading on the magnitude of APD oscillations was synergistic. (5) The presence of calcium overload and reduced repolarization reserve further enhanced the magnitude of APD oscillations and was accompanied by afterdepolarizations and/or spontaneous APs. In conclusion, low-frequency oscillations of repolarization recently reported in humans were induced by phasic β-AS and phasic mechanical loading, which acted synergistically, and were greatly enhanced by disease-associated conditions, leading to arrhythmogenic events.

Keywords

Ventricular repolarization oscillations; beta-adrenergic stimulation; mechanical stretch; calcium overload; arrhythmogenesis; computer modeling.

1. Introduction

We have recently reported that ventricular action potential (AP) duration (APD) in humans may oscillate at frequencies of the sympathetic nerve rhythm, between 0.03 and 0.15 Hz [1]. However, the mechanism underlying these phasic APD changes is at present unclear. Coherence analysis showed that the presence of these APD oscillations was related to the presence of low-frequency haemodynamic oscillations of blood pressure (BP) known as Mayer waves [1]. Changes in haemodynamic loading are well known to modulate APD through the process of mechano-electric feedback, whereby changes in myocardial stress / strain alter the electrophysiology [2]. Changes in ventricular APD in response to transient changes in ventricular loading have been demonstrated in humans [3]. Oscillations of BP at the Mayer frequency range are generally thought to be due to phasic changes in peripheral resistance and vasomotor tone [4]. Mayer waves are reduced or abolished by α-adrenergic blockade and enhanced in the presence of increased sympathetic nerve activity [4]. The above considerations therefore suggest a role of the sympathetic nerve activity in generating the APD oscillations, either directly through a β-adrenergic action and /or through the intermediary of mechano-electric coupling.

Sympathetic nerve stimulation modulates ventricular APD as a result of the net effect on a number of membrane currents, in particular the L-type calcium current (I_{CaL}) and the slowed delayed rectifier potassium current (I_{Ks}) [5]. We have used computational modelling to examine the possibility that phasic β-adrenergic stimulation (β-AS) at frequencies in the Mayer wave range might induce corresponding phasic changes in APD. Initial observations suggested that this was not the case in accordance with the slow phosphorylation and dephosphorylation kinetics of cellular protein kinase A (PKA) substrates. However, when phasic β-AS was prolonged, APD oscillations at the simulated frequency developed. In view of the relation between APD oscillations and the presence of BP oscillations (Mayer

waves) in intact humans [1], we next examined the hypothesis that APD oscillations might be secondary to BP oscillations inducing phasic changes in ventricular loading and modulating APD through changes in intracellular calcium and the opening of mechano-sensitive ion channels. As mechano-electric coupling (MEC) [2] has been shown to be potentiated by β-AS [6], we then examined the effect of cyclical haemodynamic changes in the presence of enhanced background β-AS on APD. Finally, we investigated the effect of calcium (Ca^{2+}) overload and reduced repolarization reserve (RRR), both commonly associated with disease and both well known to be pro-arrhythmic.

2. Methods

2.1 Human data

We previously reported the presence of oscillations of ventricular APD in the Mayer wave frequency range in humans [1] (Figure 1). The methodology has been described in detail in [1], in brief: 14 ambulatory patients with heart failure with biventricular pacing devices were studied while watching movie clips to enhance arousal. Unipolar electrograms were recorded from the left ventricular epicardial electrode of the device while cycle length (CL) was maintained constant by right ventricular pacing from the device. Activation recovery intervals (ARIs) were measured from electrograms as a conventional surrogate for APD [7]. BP was measured non-invasively (Finapress). Oscillations were quantified using time-frequency and coherence analysis. Oscillations in systolic (as well as diastolic) BP at the Mayer wave frequency (0.03 – 0.15 Hz) were observed in all patients. In 6 patients (43%), Mayer wave frequency oscillations were also detected in the APD (ARI). Oscillations in APD and systolic BP (diastolic BP, respectively) were significantly coupled in all patients where these could be measured.

2.2 Ventricular cell electrophysiological models

The O'Hara human ventricular AP model [8], developed based on human undiseased data, was used as a basis to represent the electrophysiology of epicardial cells. As in previous studies [9], the formulation for the fast sodium current in the O'Hara model was replaced with an alternative one, in this case adopted from the ten Tusscher human ventricular model [10], which allows for further use of the model if electrical propagation in tissue wants to be simulated.

For confirmation of some of the results obtained with the O'Hara model, the ten Tusscher human ventricular epicardial model was additionally used. Similarly to other modelling studies [11], the formulation for the Na^+/Ca^{2+} exchange current (I_{NaCa}) was taken from [12], with the parameter values reported therein, which resulted from fitting experimental data from non-failing human hearts. In contrast to

the original formulation, the utilized one includes allosteric activation by Ca^{2+}. In analogy, the same formulation for the I_{NaCa} current proposed in [12] was adopted for the O'Hara model, which originally included a mechanistically novel formulation to try to reproduce the non-failing human ventricular data presented by Weber et al. [12].

AP models representative of other animal species were additionally used in the present work to confirm simulation results in other species and verify model independence. These included the Decker model for dog [13] and the Shannon model [14] for rabbit. Also, the Negroni rabbit model integrating ionic, contractile and β-AS formulations [15] was employed for specific simulations, being its electrophysiological description based on the Shannon model. The integrative Terkildsen rat model combining the Pandit-Hinch model for the electrophysiology-Ca^{2+} dynamics with the Niederer model for the mechanics was additionally employed [16].

2.3   PKA phosphorylation

PKA phosphorylation effects were included in the models using two different approaches. The first one, defined in [17], uses subpopulations of phosphorylated and non-phosphorylated channels for each substrate affected by β-AS. At each time instant, the total current or flux was computed as a weighted average of the two subpopulations, with the fraction of phosphorylated channels being determined by the β-adrenergic cascade, as defined in [17]. The properties of the non-phosphorylated channels were described by the baseline electrophysiological model for either human or dog [8, 13], while the properties of the phosphorylated channels were determined from experimental data for a saturating dose of the β-adrenergic agonist isoproterenol (ISO), as defined in [18] for human and [17] for dog.

The second approach, defined in [19] and subsequently updated in [5, 15], describes PKA-mediated phosphorylation of cellular targets with definition of graded and dynamic phosphorylation levels. In the simulations coupling the human O'Hara AP model with the β-adrenergic signaling model updated in [5], an extension of the approach described in [20] was considered to account for additional PKA substrates. I_{Ks} phosphorylation and dephosphorylation rate constants were slowed down with respect to those used in [19] to account for recent experimental observations [21], as in [5]. PKA-mediated phosphorylation of phospholemman (PLM) was described by increasing the Na^+–K^+-ATPase (NKA) affinity for intracellular Na^+ [5]. RyR phosphorylation was defined as in [17]. In the simulations involving rabbit ventricular models [19, 15], the formulations reported in the respective studies were used, with I_{Ks} phosphorylation and dephosphorylation rate constants being also slowed down when including PKA effects in the Shannon rabbit model [19].

The two PKA phosphorylation models described above will be generally referred as Heijman and Xie models, respectively. Note that two different PKA models (one originally developed for dog and the other one for rabbit) were used to confirm that, independently of how phosphorylation effects were represented in the

models, the conclusions on the role of β-AS in modulating APD oscillations were still valid.

2.4 Electromechanical cell models

The human ventricular electrophysiological models described in 2.2 were coupled to a modified version of the Niederer active contraction model [22]. This modified version (modNiederer model) includes a description of sarcomere length (SL) variation during the cardiac cycle, developed based on physiological patterns published in the literature [23] obtained using tagged magnetic resonance images of the short and long axis of the heart during pacing [24, 25]. Similar descriptions have been used in other studies [26]. Figure S1 in the Supplementary Material shows the stretch ratio λ for this model, with λ representing SL normalized by resting SL. The modNiederer contraction model was adjusted to human cell characteristics following an approach similar to that described in [26], which involved modifications in the relaxation rates α_{r1} and α_{r2} to account for increases in these rates under higher body temperatures as well as modifications in the parameters T_{ref} and Ca_{50ref} determining contractile tension.

For confirmation purposes, the Niederer contraction model, with the same adjustments to human characteristics, was used. Additionally, a set of simulations was run with electromechanical cell models obtained from coupling human AP models with the Rice model of myofilament dynamics [27].

In the coupled electromechanical models, the free cytoplasmic Ca^{2+} concentration computed according to the electrophysiological model served as an input for the mechanical model. The mechanical model, in turn, fed back the amount of Ca^{2+} buffered to troponin, computed as a function of SL, into the electrophysiological model (details can be found in the Supplementary Material).

Finally, the integrated Negroni rabbit model [15] referred to in section 2.2 was used to investigate the joint electrical and mechanical cellular response to β-AS. In particular, the Negroni model incorporates β-AS effects on properties like myofilament Ca^{2+} sensitivity and titin stiffness as well as cross-bridge cycling rate [15]. The use of this model allows dissecting the contribution of β-AS-induced effects on myofilament properties to APD oscillatory behavior separately from the contribution of β-AS-induced effects on ionic currents and fluxes.

A list of all the combined models used in the present study integrating electrophysiological, PKA and/or mechanical formulations is presented in Table 1 together with the phenomena they are used to investigate and the reason for their introduction. The primary combined model used in this study is the O'Hara-Xie-modNiederer model. The O'Hara model is the most up-to-date human ventricular electrophysiological model, developed based on newly recorded human undiseased data. The Xie model, with incorporated updates as explained in section 2.3, describes PKA phosphorylation taking into account differential non-steady state kinetics of phosphorylation targets. The modNiederer model is based on the

mechanical Niederer model, with parameter value modifications to represent human characteristics and with incorporation of SL variation during the cardiac cycle based on physiological patterns, as described in the first paragraph of this subsection.

Several of the combined models listed in Table 1 are representative of animal species rather than human. Even if the main interest of our study is in the use of human models, also because the experimental data used for comparison comes from humans, we used animal models for confirmation of the main findings and mechanisms. Some of the utilized human models were originally developed for other species and have been subsequently adapted to human, thus corroboration of the simulated results using models specifically developed for rabbit, dog or rat provides additional value to our obtained outcomes.

2.5 Stretch-activated channels

Stretch-activated channels (SACs) were introduced in the above described electromechanical cell models. I_{SAC} was defined as the total current through both K^+-selective and non-specific cationic SACs.

Similarly to other electromechanical models published in the literature [28, 29], a linear time-independent formulation was used for the current through non-selective cationic SACs:

$$I_{SAC,ns} = G_{SAC,ns} \ ((\lambda\text{-}1)/(\lambda_{max}\text{-}1)) \ (V\text{-}E_{SAC,ns}), \qquad\qquad \text{if } \lambda > 1$$
$$I_{SAC,ns} = 0, \qquad\qquad\qquad \text{if } \lambda \leq 1$$

where λ is the ratio between SL and the resting SL defined in the model and λ_{max} is set to 1.1 as in [26, 28]. The reversal potential $E_{SAC,ns}$ was set to -10 mV based on experimental evidence [30, 31]. Provided the wide range of conductances reported for these channels, we considered both low (0.002 nS/pF) and high (0.006 nS/pF) $G_{SAC,ns}$ conductance values. Additionally, in accordance with publications reporting higher stretch-sensitivity of these channels in disease, as e.g. in hypertrophied versus control myocytes [30], $G_{SAC,ns}$ was set to 0.01 nS/pF when simulating disease conditions associated with Ca^{2+} overload or RRR. All the above $G_{SAC,ns}$ values lie within the limits reported in the literature [32, 33].

The current through K^+-selective SACs was modelled as an outwardly-rectifying current [28, 29] with parameter values obtained from the experimental fitting reported in [29]:

$$I_{SAC,K} = G_{SAC,K} \ ((\lambda\text{-}1)/(\lambda_{max}\text{-}1)) \ (1/(1+\exp((V\text{-}19.05)/29.98))), \qquad \text{if } \lambda > 1$$
$$I_{SAC,K} = 0, \qquad\qquad\qquad \text{if } \lambda \leq 1$$

The conductance $G_{SAC,K}$ was set to match experimental current values measured in epicardium [34], as in [29].

2.6 Computational simulations

Pacing protocol: Numerical experiments were performed to investigate the individual and collective effects of phasic β-AS and stretch. Virtual cells were paced

at a basic CL of 1 s, although other cycle lengths varying between 0.5 and 1.5 s were additionally explored. In each simulation, steady state initial conditions were used, which were obtained after having paced the cell at the simulated CL for a thousand beats. The stimulus current magnitude and duration were defined as originally described for each model. APD was measured at 90% repolarization.

Phasic β-AS: Phasic β-AS at a specified Mayer wave frequency ϕ between 0.03 and 0.15 Hz was simulated by stimulating the cell with isoproterenol (ISO) following periodic stepwise variations in which ISO was present at a fixed concentration during half of the Mayer wave period and was absent in the other half, in line with reported patterns of muscle sympathetic nerve activity during sympathetic activation [35]. An ISO level of 1 μM, corresponding to maximal β-AS effects, was used for the simulations, but other levels of 0.01 and 0.1 μM were also tested.

Phasic haemodynamic loading: Phasic changes in haemodynamic loading at a Mayer wave frequency ϕ were investigated using the modNiederer, Niederer and Rice mechanical models. Using the modNiederer model, simulations were run in which the end-diastolic value of the stretch ratio λ was varied along cardiac cycles following a sinusoidal waveform of frequency ϕ and maximal value of 1.1 corresponding to 10% stretch, in line with percentages tested in other studies [36]. The effect of a lower stretch level (5%) was additionally evaluated. The sinusoidal shape is in line with our experimentally observed pressure variations during sympathetic activation [1]. Additionally, simulations were run in which the end-systolic value of the stretch ratio λ was sinusoidally varied along cardiac cycles. For confirmation purposes, in a set of simulations the Rice myofilament model [27] was used and the effects of variations in SL were analysed following a similar procedure. Also, the Niederer model (not including SL variations within the cardiac cycle) was used to assess the effects of phasic sinusoidal changes in SL along time.

Combined phasic β-AS and *haemodynamic loading:* Combined phasic changes in β-AS and haemodynamic loading were evaluated, with different delays between one and the other action being defined. The range of simulated delays covered from concomitant to completely out-of-phase β-AS and stretch changes.

Mayer wave frequencies: A range of Mayer wave frequencies (0.03 - 0.15 Hz) were considered for simulation of phasic β-AS and haemodynamic loading, in accordance with the data reported in [1], of which representative sets are presented in Figure 1. Graphical results are shown in the present work for $\phi = 0.05$ Hz. Results for other frequencies, $\phi = 0.03$ Hz and 0.1 Hz, are reported in the text.

APD oscillation magnitude: In all cases where APD oscillated around a given value, the magnitude of the oscillations was quantified as the peak-to-peak amplitude of the APD series. Specifically, the peak-to-peak APD amplitude was computed in five consecutive oscillation periods and the maximum of the five amplitudes was calculated. This quantity was denoted by m_{APD}.

Simulation of disease conditions: In addition to models representing normal physiology, disease conditions associated with Ca^{2+} overload and RRR were simulated. Ca^{2+} overload was modelled by increasing the extracellular calcium

concentration (Ca_o) [37, 38] to different extents corresponding to amplification factors of 1.5, 2, 2.5 and 4. Additionally, other forms of inducing Ca^{2+} overload were simulated by attenuating the activity of the Na^+/K^+ pump through a decrease in its maximal conductance or an increase in its intracellular sodium (Na_i) half-saturation constant [39, 40, 41, 42]. RRR conditions were simulated by simultaneously inhibiting the fast and slow delayed rectifier potassium currents, I_{Kr} and I_{Ks}, [43] by up to 30% and 80%, respectively [18]. Simulations were carried out to evaluate how Ca^{2+} overload (analogously, RRR) altered the magnitude of APD oscillations and to assess whether these alterations were modulated by the interaction with the adrenergic action, the stretch action or both. Specifically, APD oscillations were induced by β-AS, stretch and the combination of the two under physiological as well as under Ca^{2+} overload (analogously, RRR) conditions and their magnitudes were compared in each case.

3. Results

3.1 Short phasic β-AS does not initiate APD oscillations at Mayer wave frequencies

Immediately following a period of enhanced β-AS, global shortening of the APD was observed. This is illustrated in Figure 2, where the upper panel shows the time series of periodic ISO application and the lower panel shows the corresponding APD response calculated with the coupled O'Hara-Xie-modNiederer model. In each 20-second period APD prolongation and shortening were observed, with the amount of APD prolongation being small compared to the more pronounced APD shortening. As can be seen from the figure, the global APD shortening trend dominated and masked concomitant oscillatory behavior in the APD.

3.2 Prolonged phasic β-AS induces low-level APD oscillations at Mayer wave frequencies

After a prolonged interval of enhanced β-AS, phosphorylation levels of all cellular substrates were seen to effectively oscillate. Figure 3A shows phosphorylation levels computed with the Heijman (left panel) and Xie (right panel) signaling models, with the specific modifications described in section 2.3. Time 0 corresponds to the start time of phasic β-AS (ISO varying between 0 and 1 μM in 20-second periods as in Figure 2). In each of the two models, large differences between the phosphorylation kinetics of modelled cellular substrates can be appreciated, with some of them, like I_{Ks}, presenting very slow trends as compared to other substrates

with very fast dynamics. This underlies the fact that the APD takes some time (3-4 minutes) to start oscillating following enhanced β-AS.

The effects of prolonged phasic β-AS on human ventricular APD are presented in Figure 3B for the O'Hara-Xie-modNiederer model. APD oscillations of 4-5 ms in magnitude developed in response to prolonged phasic changes in ISO concentration. Phosphorylation levels of PKA targets are presented together with the three currents associated with the targets having the largest contribution to APD, particularly I_{CaL} and I_{Ks}. While all substrates oscillated with a 20-second period, phosphorylation-induced increase in I_{CaL} absolute magnitude following each ISO application was faster than the corresponding increase in I_{Ks} (Figure 3B, insets). This mechanism underlies the initial APD prolongation observed at the beginning of each β-AS period (ISO varying from 0 to 1), which was subsequently followed by APD shortening as I_{Ks} phosphorylation started taking more relevance. Similarly, faster changes in I_{CaL} as compared to I_{Ks} upon ISO returning to 0 (Figure 3B, insets) served to explain early APD shortening followed by successive prolongation.

Prolonged phasic β-AS induced APD oscillations also for other AP models and PKA formulations. For the O'Hara-Heijman-modNiederer model, the magnitude of human APD oscillations was 2-3 ms, although the kinetics during the first minutes after the start of phasic β-AS were substantially different from those of the O'Hara-Xie-modNiederer model due to differences between the Heijman and Xie phosphorylation descriptions (Figure 3A). For coupled electrophysiological and β-adrenergic signalling models representative of other animal species, the magnitude of the oscillations induced by prolonged phasic β-AS varied from 2 ms for the canine Decker-Heijman model to 8 ms for the rabbit Shannon-Soltis model.

Additionally, the dependence of APD oscillations' characteristics on the pacing frequency and on β-AS frequency and strength were tested. In all cases APD oscillations could be appreciated, with their magnitude increasing for larger ISO concentrations (β-AS strength) and decreasing for higher pacing and β-AS frequencies. An oscillation range was quantified for the O'Hara-Xie-modNiederer model, spanning from 1 ms for a pacing CL of 0.5 s, Mayer wave frequency of 0.1 Hz and ISO concentration of 0.01 μM to 7 ms for corresponding values of 1.5 s CL, 0.03 Hz Mayer frequency and 1 μM ISO. This range of APD oscillations lies within the values reported in [1] for low-frequency ARI oscillations evoked by mental arousal, covering the low to middle reported range.

Results corresponding to assessment of whether β-AS effects on myofilament properties could add to the magnitude of APD oscillations observed after prolonged phasic stimulation are presented in Figure 4. As illustrated in the figure, for APs calculated with the Negroni model, removing ISO effects from myofilaments led to APD oscillations of a magnitude comparable to that obtained when ISO effects on all ion fluxes and myofilaments were included (5.4 vs 5.8 ms). While a number of alterations could be observed after removing ISO effects on myofilaments, including a reduction in peak systolic calcium, preservation of peak force and an increase in

contraction duration (Figure 4, lower three panels), this only had a minor impact on APD fluctuations (Figure 4, second upper panel). It is also interesting to note that, even if this model reproduces the ISO-induced APD shortening reported experimentally at steady state, a transient APD prolongation lasting for more than 10 seconds occurred following each ISO application. This explains why after a prolonged interval of phasic β-AS, the APD lengthened during each ISO phase and, analogously, shortened during the phase of ISO absence (Figure 4, second upper panel).

3.3 Phasic stretch changes contribute to APD oscillations at Mayer wave frequencies

Simulation of phasic changes in SL, associated with changes in haemodynamic loading accompanying enhanced sympathetic activity, led to almost immediate oscillations in the APD. Figure 5 presents the results of simulating 20-second period variations in end-diastolic SL for the O'Hara-Xie-modNiederer model in the absence of β-AS. Three different results are shown, corresponding to two cases where SACs are included in the model and one case where SACs are not modelled. When SAC effects were not considered (Figure 5, black line), stretch (represented by the stretch ratio λ in the first panel) increased the amount of Ca^{2+} bound to troponin C (Ca_{Trop}, third panel) and decelerated the decay of such a concentration. This, in turn, caused a reduction in the free cytosolic Ca^{2+} concentration (fourth panel) and, as a consequence, there was an increase in the outward (reverse-mode) and a decrease in the inward (forward-mode) Na^+/Ca^{2+} exchanger current (I_{NaCa}, fifth panel). All together those alterations led to APD shortening (second panel). Similarly, distension led to APD prolongation. Therefore, APD oscillated with the same 20-second period in response to phasic 10% stretch changes, being the magnitude of the oscillations of around 7 ms. To confirm that these observations were independent of the employed electrophysiological model, the simulation was repeated using the ten Tusscher human ventricular model coupled to the same modNiederer active contraction model. APD oscillations of 6 ms were observed and the aforementioned mechanisms were corroborated, thus confirming independence of the chosen model. Additionally, the Terkildsen rat model was shown to yield similar results in terms of stretch-induced APD oscillations and associated mechanisms, with the only difference being the lack of stretch-induced changes in the outward I_{NaCa} current despite a similar reduction in inward I_{NaCa}. In this rat model the maximum amplitude of APD oscillations was of 8 ms.

The contribution of SACs to APD oscillations was assessed for low (G_L = 0.002 nS/pF) and high (G_H = 0.006 nS/pF) conductance non-selective cation channels. The stretch-induced changes in Ca^{2+} dynamics and I_{NaCa} current tended to shorten the APD, an effect that in the G_L case was magnified after introducing I_{SAC} as a result of the large outward current through $I_{SAC,K}$ and partially through $I_{SAC,ns}$ (Figure 5, green line). The magnitude of APD oscillations in that case increased up to 10.0 ms. In the

G_H case (Figure 5, red line), however, the inward current through non-cation SACs became substantially more relevant and contributed to stretch-induced APD prolongation, overcoming the shortening effect induced by stretch in the absence of I_{SAC}. In this case, the APD oscillation magnitude was as high as 11.8 ms.

In addition to the effect of non-selective SAC conductance, the magnitude of low-frequency APD oscillations was also found to be dependent on the stretch level. For 5% stretch, APD fluctuations spanned from 3.6 ms to 5.0 ms, depending on the value of $G_{SAC,ns}$. The variability in the magnitude of APD oscillations for simulated 5% and 10% stretch levels and different SAC conductances is in line with the wide spectra of APD fluctuations reported in [1] (see e.g. Figure 1).

Furthermore, the effect of varying end-systolic SL shortening was assessed using the O'Hara-Xie-modNiederer model. Results confirmed that, in agreement with previous experimental observations [44], the impact on APD oscillations was little (below 2 ms) even for large simulated variations.

The reported results on the contribution of haemodynamic loading changes to APD oscillatory behavior were confirmed by coupling the human ventricular AP models (O'Hara and ten Tusscher models) with the Niederer model and/or the Rice myofilament model. Phasic sinusoidal changes in end-diastolic sarcomere length led to almost immediate APD oscillations, in agreement with the results obtained when the modNiederer model was used. For 10% stretch, the Niederer and modNiederer models led to similar magnitudes of APD oscillations (differences up to 1 ms), while the Rice myofilament model provided lower APD oscillation magnitudes than the modNiederer model (up to 5 ms below depending on $I_{SAC,ns}$ conductance). Simulation results using coupled electro-mechanical models with the Rice description for myofilament dynamics additionally confirmed that varying end-systolic SL shortening very slightly altered the APD (magnitude of APD oscillations less than 2 ms).

3.4 Combined phasic β-AS and stretch potentiate APD oscillations at Mayer wave frequencies

Phasic β-AS and stretch concurred to amplify the magnitude of APD oscillations. Figure 6A shows APD oscillations (bottom panel), calculated with the O'Hara-Xie-modNiederer model, arising after a period of prolonged phasic β-AS (top panel) and stretch changes (middle panel). Both effects were simulated as periodic and concurrent in time, meaning that changes in ISO concentration started at the same time as those in the stretch ratio. The mechanisms underlying ISO-induced and stretch-induced electrophysiological alterations, described in 3.2 and 3.3, were observed to act synergistically to produce larger APD fluctuations.

The comparison between the individual effects of prolonged β-AS (Figure 3B), individual stretch changes (Figure 5) and the combination of β-AS and stretch (Figure 6A) are summarized in Figure 6B for the O'Hara-Xie-modNiederer model. When SACs were not incorporated into the model, the magnitude of β-AS-induced

APD oscillations was lower than that of stretch-induced ones and the conjunction of the two effects led to fluctuations of amplitude clearly larger than the individual amplitudes. In the presence of SACs the conjunction of β-AS and stretch enhanced the individual contributions or, at least, approximately maintained the largest one of the two (see Figure 6B). The same conclusion was reached when using the Niederer model instead of the modNiederer model.

The temporal coordination of the two actions, β-AS and stretch, modulated APD oscillatory behavior. When β-AS and stretch acted in phase inducing APD oscillations that followed a similar temporal pattern (i.e. they induced simultaneous APD prolongation and shortening), a delay in one of the actions with respect to the other desynchronized the APD oscillations and resulted in a reduction in the oscillation amplitude. This occurred in the absence of SACs (where the reduction went from 9 ms for no delay to 7.5 ms for a 10-second delay) and in the case of SACs with G_L conductance (with a reduction from 9.6 ms to 7.5 ms). However, in the case of SACs with G_H conductance, an amplification of the individual effects was observed because a 10-second delay acted to synchronize the oscillations induced by β-AS and stretch (the oscillation magnitude varied from 11.9 ms to 17.6 ms). Similar results for concomitant and out-of-phase β-AS- and stretch-induced APD oscillations were observed with other models.

Of note, the above reported ranges of low-frequency APD oscillations due to the combination of phasic β-AS and stretch changes are still in accordance with the APD fluctuation amplitudes reported in [1], examples of which are illustrated in Figure 1.

3.5 Disease-related conditions involving calcium overload and reduced repolarisation reserve lead to magnification of APD oscillations and instabilities

Low-frequency APD fluctuations induced by phasic β-AS and/or stretch were potentiated in Ca^{2+} overloaded myocytes. Figure 7A shows Δ APD under different levels of Ca^{2+} overload, with Δ APD calculated as a difference of each APD with respect to the minimum APD value. The presented results were obtained following prolonged phasic β-AS and stretch as in Figure 6A, using the O'Hara-Xie-modNiederer model with $G_{SAC,ns}$ set to G_H. As illustrated in the graphic, the higher the level of Ca^{2+} overload, the larger the oscillation magnitude.

Our results showed that Ca^{2+} overloaded enhanced APD oscillations due to adrenergic stimulation as well as stretch. When produced as a result of stretch, this effect was amplified after including the contribution of SACs. Following an increase in extracellular Ca^{2+}, changes in Ca^{2+} bound to troponin, free cytosolic Ca^{2+}, I_{Ks}, I_{CaL}, I_{NaK} or I_{NaCa} were observed. The magnitude of APD oscillations increased as a result of the variation in these currents and fluxes.

Other approaches used for simulation of Ca^{2+} overload conditions, involving alterations in the activity of the Na^+/K^+ pump as described in section 2.6, led to very similar conclusions in terms of potentiation of APD oscillations as compared to physiological conditions. Illustration of the enhancement of APD oscillation magnitude under Ca^{2+} overload conditions simulated with those other approaches is provided in Figure S2 of the Supplementary Material. In this case, the magnification observed in Ca^{2+} overloaded myocytes was also more notable for stretch-induced oscillations after incorporating SACs into the models.

RRR had a parallel impact on low-frequency APD fluctuations. Similarly to Figure 7A, Figure 7B shows Δ APD induced by prolonged phasic β-AS and stretch under increasing degrees of I_{Kr} and I_{Ks} inhibition, which in turn led to gradually larger magnitudes of APD oscillation. Under RRR conditions, the magnification of APD oscillations was observed both when these were induced by β-AS or by stretch. Inhibition of the I_{Kr} current was identified as an important mechanism whereby RRR enhanced APD oscillations. I_{Kr} inhibition notably prolonged the AP and accentuated the contribution of other currents, like I_{Ks} or I_{SAC}, to APD fluctuations in response to both phasic β-AS and stretch. In fact, simulation of RRR via inhibition of solely I_{Ks} by up to 80% did not result in any remarkable enhancement of APD oscillations, which maintained a magnitude similar to that under physiological conditions in response to β-AS, stretch (in the presence of SACs) or the combination of both. These results confirm that in those cases where I_{Ks} or $I_{SAC,K}$ are important drivers of APD oscillations, inhibition of I_{Kr} acts to potentiate their contribution.

The combination of Ca^{2+} overload and RRR induced APD oscillations of larger magnitude than when RRR and Ca^{2+} overload were evaluated separately. Figure 7C summarizes the results corresponding to 20-second period APD oscillations induced by phasic β-AS and stretch under physiological conditions, Ca^{2+} overload (simulated by increasing Ca_o by a factor of 2.5), RRR (simulated by inhibiting I_{Kr} by 22.5 % and I_{Ks} by 60%) and the combination of the two latter ones.

The enhancement of APD oscillations in Ca^{2+} overloaded and RRR myocytes was also observed for other coupled models. When the Heijman description for PKA phosphorylation of cellular substrates was used, phasic β-AS and stretch generated large APD fluctuations under concurrently simulated Ca^{2+} overload and RRR, as described above, subsequently leading to early afterdepolarisations (EADs). The observed afterdepolarizations were facilitated by the large current through non-selective SACs, which contributed to augmentation of the net inward current and AP prolongation during repolarization. The main mechanism for EAD generation was reactivation of the I_{CaL} current. The I_{NaCa} current, however, changed to the outward direction during the EAD depolarization, thus not contributing to its initiation. Confirmation of the I_{CaL} role in EAD generation was provided by e.g. blockade of I_{CaL}, which completely abolished EADs. Our observed mechanisms are in line with those reported for EAD triggering in other scenarios [45, 46].

When on top of RRR and Ca^{2+} overload, the conductance of non-selective SACs increased ($G_{SAC,ns}$ equal to 0.01 nS/pF), as reported for disease conditions

[30], further electrical abnormalities were observed. Figure 8 compares the effects of continuous (top panel) vs phasic (bottom panel) β-AS, the latter additionally accompanied by phasic stretch changes. Transmembrane voltage was computed with the O'Hara-Xie-modNiederer model under the same high levels of Ca^{2+} overload and RRR in the two cases. APs before the start of β-AS are presented in the left column for comparison. After a brief period of β-AS, irregularities in the repolarising phase of the AP appeared when stimulation was phasic and accompanied by stretch, but not when stimulation was continuous (middle column). A prolonged period of phasic, not continuous, stimulation led to EADs and EAD bursts (right column). As described in the paragraph above, the current through non-selective SACs augmented the net inward current and prolonged the AP, thus facilitating I_{CaL} reactivation.

Other coupled models used in the present study further corroborated the occurrence of electrical abnormalities induced by phasic β-AS and/or stretch under Ca^{2+} overload and RRR. Using the Negroni model, delayed afterdepolarizations (DADs) and spontaneous APs could be observed at increased Ca_o levels and reduced I_{Kr} and I_{Ks} currents. These were the result of myocyte's Ca^{2+} overloading, which triggered an abnormal release of Ca^{2+} from the sarcoplasmic reticulum and activated the inward Na^+/Ca^{2+} exchanger current to generate DADs and extra APs. Phasic β-AS accompanied by phasic stretch largely facilitated the occurrence of such abnormalities, as compared to constant β-AS, by lowering the levels of Ca^{2+} overload and RRR at which DADs and extra APs started to appear.

4.   Discussion

We have investigated the cellular mechanisms underlying phasic modulation of ventricular APD within the 0.03-0.15 Hz sympathetic nerve frequency, as recently reported in humans in vivo [1], using computational modelling. We employed cellular models coupling descriptions of ventricular electrophysiology, β-adrenergic signalling and mechanical contraction, mostly for human but also for other species like rabbit and dog. By using different models of human and other animal species we demonstrated that the presented results were largely model-independent. The main findings were: (1) Following the onset of phasic β-AS, a progressive decrease in APD was observed together with concomitant small APD oscillations. However, if phasic β-AS was continued for more than 3-4 minutes, APD oscillations at the β-AS frequency became apparent; (2) Phasic mechanical stretch at Mayer wave frequencies, simulating haemodynamic variations accompanying enhanced sympathetic activity, immediately resulted in APD oscillations; (3) The combination of phasic β-AS and mechanical stretch resulted in synergistic enhancement of APD oscillation; (4) In the presence of Ca^{2+} overload the magnitude of APD oscillation in response to combined phasic β-AS and mechanical stretch was enhanced in a dose

dependent manner, and further enhanced with the addition of RRR (reduced I_{Kr} and I_{Ks}); (5) Electrical abnormalities in the form of afterdepolarizations and spontaneous APs were induced by phasic β-AS and stretch in myocytes with high levels of Ca^{2+} overload and RRR.

Periodic repolarization dynamics at Mayer wave frequencies have recently been reported in a swine model and in humans [47]. On the basis of the known organization of sympathetic activity in a series of low frequency bursts [48, 35, 49] the authors examined the hypothesis that phasic sympathetic activation induces phasic changes in repolarization localized in the low-frequency spectral range. Using a measure of repolarization derived from the conventional electrocardiographic T wave they demonstrated periodic oscillation of repolarization at this frequency, which was enhanced by sympathetic activation and reduced by sympathetic blockade [47]. We have recently reported the presence of low-frequency oscillations at the level of the ventricular APD (measured as ARIs from unipolar electrograms) in ambulatory patients with heart failure during enhanced sympathetic activity [1]. In these patients, the presence of an implanted resynchronization device for biventricular pacing enabled recordings to be obtained directly from the left ventricular epicardium while simultaneously controlling cycle length with right ventricular pacing. We are not aware of other studies in the literature, either in animal models or in humans, describing synchronization between ARI variations and Mayer waves.

Experimentally, the effect of sustained β-AS is usually to shorten ventricular APD, although both APD increases and decreases have been reported [50, 51, 52]. A biphasic effect has recently been reported with an initial lengthening of APD followed after a few seconds by APD shortening [53, 21]. The initial lengthening was attributed to an early dominant effect of I_{CaL} due to its more rapid onset kinetics, and the subsequent shortening due to the slower activating I_{Ks} [5, 53]. The initial effect of phasic β-AS in our simulations was a global trend of progressive APD shortening with alternate APD increases and decreases in response to the periodic β-AS, being the APD decreases much larger than the increases. Following each β-AS application, the APD initially prolonged during a few beats and subsequently shortened, in agreement with the above described experimental observations. The absence of oscillations around a fixed APD value is consistent with the slow phosphorylation and dephosphorylation kinetics of cellular PKA substrates. However, when phasic β-AS was prolonged, APD oscillations developed after 3-4 minutes, the time by which most PKA phosphorylation targets already reached its maximal phosphorylation level and started fluctuating around it. Our results are in good correspondence with the fact that, departing from basal conditions, enhanced β-AS has a large impact on ventricular electrophysiology, while after a period of prolonged β-AS adrenoceptors become less sensitive to the same stimulus than when they were in their basal state.

The association that we observed between APD oscillations at 0.03-0.15 Hz frequencies and the presence of BP oscillations at the same frequency (Mayer waves) in humans [1] raises the possibility that MEC may play a role in the phasic

modulation of APD. Oscillations in BP would be expected to reflect phasic changes in haemodynamic loading on the ventricular myocardium which may in turn influence APD on a beat-to-beat basis [2, 3]. The effect of MEC on APD is complex, depending on the nature of mechanical stretch / strain on the myocardial fibers, its timing in relation to the time course of AP repolarization and the extent of fiber excursion, and involving several cellular mechanisms including calcium cycling and SACs [54, 32, 55, 56, 57]. We simulated MEC by building biophysical models coupling electrophysiology and mechanics that include both direct and feedback mechanisms. In these models, the Ca^{2+} transient calculated from the electrophysiological model was the input for the mechanical model (direct pathway). In turn, the mechanical model was used to update Ca^{2+} dynamics as a function of the amount of Ca^{2+} bound to troponin C and, additionally, the current through SACs was incorporated into the ionic model subject to the stretch level defined in the mechanical model (feedback pathway). Using the described electro-mechanical models, APD oscillations at the same frequency of stretch-induced changes were established. Our simulations showed an additive effect of phasic β-AS and MEC on the magnitude of APD oscillations consistent with the known potentiating effect of β-AS on mechanically induced changes in APD [6]. The mechanisms underlying APD oscillations under individual β-AS and stretch actions remained valid when the combination of the two was simulated, thus adding to the oscillation magnitude.

Two commonly associated properties of the hearts of patients with ischemic heart disease, post myocardial infarction and cardiac failure are the presence of cellular Ca^{2+} overload and RRR [58]. Both are known to promote the development of afterdepolarizations and be pro-arrhythmic [58]. Our results showed that the presence of Ca^{2+} overload enhances the magnitude of APD oscillations induced by phasic β-AS and MEC. The magnitude of APD oscillations were further enhanced by the additional presence of RRR. This additional enhancement is related to the fact that loss of I_{Kr} in myocytes with simulated RRR allows uncovering the role of other currents, like I_{Ks} or I_{SAC}, which notably contribute to APD oscillations induced by phasic β-AS, MEC or combined β-AS and MEC. Our results on the relationship between enhanced repolarization variability and arrhythmogenesis in diseased hearts are in accordance with ECG studies showing an association between increased heart rate-compensated QT variability and arrhythmic risk [59, 60, 61]. It should be noted that in our study, as well as in the experimental data presented in [1], there is no additional contribution of heart rate variability, as CL was kept constant.

Methodological considerations

Phasic β-AS and haemodynamic loading effects were simulated following stepwise and sinusoidal temporal patterns, respectively, in line with experimentally reported patterns of variation for muscle sympathetic nerve activity and blood

pressure during sympathetic activation [35, 1]. Other types of temporal patterns of variation for simulated phasic β-AS and haemodynamic loading were tested (not shown), with the findings described in the present study remaining valid in all cases and only minor quantitative differences observed. Regarding the interaction of the two effects, phasic β-AS and myocardial stretch, simulations ranging from in-phase to completely out-of-phase cases were run and confirmation was obtained that the APD oscillations induced by one of the effects were not cancelled out by the other effect and, in most cases, the interaction was synergistic.

Ca^{2+} overload conditions were simulated by three different means (involving increased Ca$_o$ [37, 38] and reduced activity of the Na$^+$/K$^+$ pump [39, 40, 41, 42]) and in all cases magnification of APD oscillations was observed. The electrophysiological models used for these analyses, including the O'Hara and ten Tusscher human ventricular AP models [8, 10], led to APD prolongation in response to increased Ca$_o$. Future studies could explore whether the use of electrophysiological models showing APD shortening following increased Ca$_o$ [62] still support the conclusions of the present study regarding magnified APD oscillations in Ca^{2+} overloaded myocytes.

RRR was simulated by inhibition of both I$_{Kr}$ and I$_{Ks}$ currents and amplification of APD oscillations was noted. However, if RRR had been simulated by inhibition of solely I$_{Ks}$, APD oscillations of similar magnitude to those under physiological conditions had been observed for most of the simulated cases, i.e. in response to phasic β-AS, stretch in the presence of SACs and the combination of both.

The present study was limited to single cells. Further studies should extend it by including tissue simulations built on the cellular simulations here presented. This would help to clarify how the mechanisms described in this study contribute to the electrical activity at the ventricular tissue level. Nevertheless, disease conditions like myocardial ischemia and heart failure result in cell-to-cell uncoupling and in those cases the results obtained in tissue would be expected to be closer to those in single cells, as investigated in this study.

The experimental protocol used to record the human data used as a basis for the comparisons in this study [1] is known to induce heterogeneity in mechanical behavior throughout the left ventricle [24]. The left ventricular epicardial electrode used to record the unipolar electrograms is thus likely to experience notable pre-stretch and larger than normal shortening. A potential increase in myocardial strain, on top of the emotionally-induced arousal elicited by watching movies, may have facilitated a rise in the observed magnitude of the low-frequency APD oscillations quantified in [1].

Implications

Enhanced sympathetic activity is well known to be a major factor in arrhythmogenesis [63, 64]. Mechanisms include destabilization of repolarization and the generation of afterdepolarizations, and inhomogeneous changes of APD and refractoriness facilitating re-entrant arrhythmias. Oscillatory phenomena affecting the

time course of ventricular repolarization are known to predispose to ventricular tachycardia and fibrillation [65, 58]. In this study, we have described mechanisms whereby sympathetic activity contributes to the establishment of pro-arrhythmic conditions through electromechanical interactions. While the results of this computational investigation must be considered of a somewhat preliminary nature, they nevertheless suggest that oscillations in ventricular APD at Mayer wave frequencies may play a role in arrhythmogenesis. In support of this suggestion is the result of two recently reported large patient cohorts showing that increased oscillatory behavior of ventricular repolarization at those frequencies, measured at the level of the ECG, was a strong predictor of cardiovascular mortality [47]. In one large cohort of post myocardial infarction patients it was the strongest single risk predictor of total mortality [47].

When extrapolating to the clinical situation several factors need to be taken into consideration. While oscillatory behavior is an inherent feature of sympathetic nerve activity over a range of frequencies [66], the physiological regulation of the Mayer waves engages other neurocardiovascular axes in addition to sympathetic regulation, which may contribute to haemodynamic and electrophysiological oscillations. For example, Mayer waves have been attributed to a central oscillator and/or to result from delay in the baroreflex loop [67, 68, 4]. A complex interaction has been shown to occur between Mayer wave oscillations, central respiratory drive and vagal nerve activity at the level of the brain stem nuclei [69].

Studies in an ambulatory canine model of sudden death have shown an increase in sympathetic nerve activity prior to the onset of ventricular tachycardia and ventricular fibrillation [70]. Malignant ventricular arrhythmias were preceded by a progressive increase in low amplitude burst discharge and high amplitude spike discharge. Several of the illustrated examples of integrated nerve activity from that study show the presence of oscillations at the 10-second frequency [70] (Figures 4D and 4E, Figure 3B). However, several of the recordings do not show 10-second oscillation and the neural pattern preceding arrhythmias appears variable. We would propose that enhanced sympathetic activity may generate arrhythmias by several mechanisms such as described by Johnson et al. [71] and that oscillatory activity of APD when present may play a complementary role.

Studies in isolated myocytes and computer simulations during reduced repolarization reserve have shown that β-AS-induced calcium overload enhanced beat-to-beat APD variability and led to the development of early afterdepolarizations. [72, 71]. The mechanism was through intermittent spontaneous sarcoplasmic calcium release resulting in APD prolongation of the following beat due to reduced calcium deactivation of I_{CaL}. These results suggest a random process underlying the development of early afterdepolarizations rather than an oscillatory process. However, in our studies while reduced repolarization reserve and β-AS-induced calcium overload were prerequisites for EAD development, a critical factor was the on / off nature of the stimulation. For example, if basal conditions are simulated and a sudden change in β-AS and stretch applied, EADs only occur during the initial

transition, but, even if β-AS and stretch are continued, EADs no longer occur. In the case of phasic stimulation (β-AS and stretch), sudden changes in stimulation are continually applied and EADs perpetuate. The underlying mechanism relates to the different on / off time constants of calcium and potassium currents. We would envisage that the mechanisms described by Johnson et al. [71] and the phasic responses we describe here could coexist and act synergistically. Furthermore, it is generally considered that a function of oscillatory sympathetic nerve activity may be to create dynamic synchronization at effector end organs [73, 67]. It is possible therefore that oscillatory behavior of APD may produce spatio-temporal synchronization known to be important to overcome source sink mismatch and facilitate propagation of EADs [74].

5. Disclosures

The authors have nothing to disclose.

Acknowledgments

References

[1]   Hanson B, Child N, Van Duijvenboden S, Orini M, Chen Z, Coronel R, Rinaldi CA, Gill JS, Gill JS, Taggart P. Oscillatory behavior of ventricular action potential duration in heart failure patients at respiratory rate and low frequency. Front Physiol 2014;5:414.

[2]   Lab MJ. Contraction–excitation feedback in myocardium. Physiological basis and clinical relevance. Circ Res 1982;50:757-66. Review.

[3]   Taggart P, Sutton PM. Cardiac mechano-electric feedback in man: clinical relevance. Prog Biophys Mol Biol 1999;71:139-54.

[4]   Julien C. The enigma of Mayer waves: Facts and models. Cardiovasc Res 2006;70:12-21.

[5]   Xie Y, Grandi E, Puglisi JL, Sato D, Bers DM. β-adrenergic stimulation activates early afterdepolarizations transiently via kinetic mismatch of PKA targets. J Mol Cell Cardiol 2013;58:153-61.

[6]   Horner SM, Murphy CF, Coen B, Dick DJ, Lab MJ. Sympathomimetic modulation of load-dependent changes in the action potential duration in the in situ porcine heart. Cardiovasc Res 1996;32:148-57.

[7]   Coronel R, de Bakker JM, Wilms-Schopman FJ, Opthof T, Linnenbank AC, Belterman CN, Janse MJ.   Monophasic action potentials and activation recovery intervals as measures of ventricular action potential duration: experimental evidence to resolve some controversies. Heart Rhythm 2006;3:1043-50.

[8]   O'Hara T, Virág L, Varró A, Rudy Y. Simulation of the undiseased human cardiac ventricular action potential: model formulation and experimental validation. PLoS Comput Biol 2011;7:e1002061.

[9]   Deo M, Ruan Y, Pandit SV, Shah K, Berenfeld O, Blaufox A, Cerrone M, Noujaim SF, Denegri M, Jalife J, Priori SG. KCNJ2 mutation in short QT syndrome 3 results in atrial fibrillation and ventricular proarrhythmia. Proc Natl Acad Sci U S A. 2013;110:4291-6.

[10]   ten Tusscher KH, Panfilov AV.   Alternans   and   spiral   breakup   in   a human ventricular tissue   model.   Am   J   Physiol Heart Circ   Physiol 2006;291:H1088-100.

[11]   Xia L, Zhang Y, Zhang H, Wei Q, Liu F, Crozier S. Simulation of Brugada syndrome   using   cellular   and   three-dimensional   whole-heart   modeling approaches. Physiol Meas 2006;27:1125-42.

[12]   Weber CR, Piacentino V 3rd, Houser SR, Bers DM. Dynamic regulation of sodium/calcium   exchange   function   in   human   heart   failure.   Circulation 2003;108:2224-9.

[13]   Decker KF, Heijman J, Silva JR, Hund TJ, Rudy Y. Properties and ionic mechanisms of action potential adaptation, restitution, and accommodation in canine epicardium. Am J Physiol Heart Circ Physiol 2009;296:H1017-26.

[14]   Shannon TR, Wang F, Puglisi J, Weber C, Bers DM. A mathematical treatment of integrated Ca dynamics within the ventricular myocyte. Biophys J 2004;87:3351-71.

[15]   Negroni JA, Morotti S, Lascano EC, Gomes AV, Grandi E, Puglisi JL, Bers DM. β-adrenergic effects on cardiac myofilaments and contraction in an integrated rabbit ventricular myocyte model. J Mol Cell Cardiol 2015;81:162-75.

[16]   Terkildsen JR, Niederer S, Crampin EJ, Hunter P, Smith NP. Using Physiome standards to couple cellular functions for rat cardiac excitation-contraction. Exp Physiol 2008;93:919-29.

[17]   Heijman J, Volders PG, Westra RL, Rudy Y. Local control of β-adrenergic stimulation: Effects on ventricular myocyte electrophysiology and Ca(2+)-transient. J Mol Cell Cardiol 2011;50:863-71.

[18]   O'Hara T, Rudy Y. Arrhythmia formation in subclinical ("silent") long QT syndrome requires multiple insults: quantitative mechanistic study using the KCNQ1 mutation Q357R as example. Heart Rhythm 2012;9:275-82.

[19] Soltis AR, Saucerman JJ. Synergy between CaMKII substrates and β-adrenergic signaling in regulation of cardiac myocyte Ca(2+) handling. Biophys J 2010;99:2038-47.

[20] Dai L, Zang Y, Zheng D, Luo R, Xia L. Modelling the integrated regulation role of β-adrenergic signaling and CaMKII in human myocyte electrophysiological properties. Proc Computing in Cardiology Conference 2013; 382-92.

[21] Liu GX, Choi BR, Ziv O, Li W, de Lange E, Qu Z, Koren G. Differential conditions for early after-depolarizations and triggered activity in cardiomyocytes derived from transgenic LQT1 and LQT2 rabbits. J Physiol 2012;590:1171-80.

[22] Niederer SA, Hunter PJ, Smith NP. A quantitative analysis of cardiac myocyte relaxation: a simulation study. Biophys J 2006;90:1697-722.

[23] Kerckhoffs RC, Bovendeerd PH, Kotte JC, Prinzen FW, Smits K, Arts T. Homogeneity of cardiac contraction despite physiological asynchrony of depolarization: a model study. Ann Biomed Eng 2003; 31:536-47.

[24] Prinzen FW, Hunter WC, Wyman BT, McVeigh ER. Mapping of regional myocardial strain and work during ventricular pacing: experimental study using magnetic resonance imaging tagging. J Am Coll Cardiol 1999;33:1735-42.

[25] Wyman BT, Hunter WC, Prinzen FW, McVeigh ER. Mapping propagation of mechanical activation in the paced heart with MRI tagging. Am J Physiol 1999;276:H881–91.

[26] Weise LD, Panfilov AV. A discrete electromechanical model for human cardiac tissue: effects of stretch-activated currents and stretch conditions on restitution properties and spiral wave dynamics. PLoS One 2013;8:e59317.

[27] Rice JJ, Wang F, Bers DM, de Tombe PP. Approximate model of cooperative activation and crossbridge cycling in cardiac muscle using ordinary differential equations. Biophys J 2008;95:2368-90.

[28] Benoist D, Stones R, Benson AP, Fowler ED, Drinkhill MJ, Hardy ME, Saint DA, Cazorla O, Bernus O, White E. Systems approach to the study of stretch and arrhythmias in right ventricular failure induced in rats by monocrotaline. Prog Biophys Mol Biol 2014;115:162-72.

[29] Healy SN, McCulloch AD. An ionic model of stretch-activated and stretch-modulated currents in rabbit ventricular myocytes. Europace 2005;7:128-34.

[30] Kamkin A, Kiseleva I, Isenberg G. Stretch-activated currents in ventricular myocytes: amplitude and arrhythmogenic effects increase with hypertrophy. Cardiovasc Res 2000;48:409-20.

[31] Isenberg G, Kazanski V, Kondratev D, Gallitelli MF, Kiseleva I, Kamkin A. Differential effects of stretch and compression on membrane currents and [Na+]c in ventricular myocytes. Prog Biophys Mol Biol 2003;82:43-56. Review.

[32] Kohl P, Hunter P, Noble D. Stretch-induced changes in heart rate and rhythm: clinical observations, experiments and mathematical models. Prog Biophys Mol Biol 1999;71:91-138. Review.

[33] Kohl P, Day K, Noble D. Cellular mechanisms of cardiac mechano-electric feedback in a mathematical model. Can J Cardiol 1998;14:111-9.

[34] Tan JH, Liu W, Saint DA. Differential expression of the mechanosensitive potassium channel TREK-1 in epicardial and endocardial myocytes in rat ventricle. Exp Physiol 2004;89:237-42.

[35] Pagani M, Montano N, Porta A, Malliani A, Abboud FM, Birkett C, Somers VK. Relationship between spectral component of cardiovascular variabilities and direct measures of sympathetic nerve activity in humans. Circulation 1997;95:1441-48.

[36] Iribe G, Kaneko T, Yamaguchi Y, Naruse K. Load dependency in force-length relations in isolated single cardiomyocytes. Prog Biophys Mol Biol 2014; 115:103-14.

[37] Venetucci LA, Trafford AW, O'Neill SC, Eisner DA. The sarcoplasmic reticulum and arrhythmogenic calcium release. Cardiovasc Res 2008;77:285-92.

[38] Wasserstrom JA, Shiferaw Y, Chen W, Ramakrishna S, Patel H, Kelly JE, O'Toole MJ, Pappas A, Chirayil N, Bassi N, Akintilo L, Wu M, Arora R, Aistrup GL. Variability in timing of spontaneous calcium release in the intact rat heart is determined by the time course of sarcoplasmic reticulum calcium load. Circ Res 2010;107:1117-26.

[39] Sulman T, Katsnelson LB, Solovyova O, Markhasin VS. Mathematical modeling of mechanically modulated rhythm disturbances in homogeneous and heterogeneous myocardium with attenuated activity of na+ -k+ pump. Bull Math Biol 2008;70:910-49.

[40] Fink M, Noble PJ, Noble D. Ca^{2+}-induced delayed afterdepolarizations are triggered by dyadic subspace $Ca2^{2+}$ affirming that increasing SERCA reduces aftercontractions. Am J Physiol Heart Circ Physiol 2011;301.H921-35.

[41] Nieman CJ, Eisner DA. Effects of caffeine, tetracaine, and ryanodine on calcium-dependent oscillations in sheep cardiac Purkinje fibers. J Gen Physiol 1985;86:877-89.

[42] Katsnelson LB, Sulman T, Solovyova O, Markhasin VS. Role of myocardial viscoelasticity in disturbances of electrical and mechanical activity in calcium overloaded cardiomyocytes: mathematical modeling. J Theor Biol 2011;272:83-95.

[43] Odening KE, Hyder O, Chaves L, Schofield L, Brunner M, Kirk M, Zehender M, Peng X, Koren G. Pharmacogenomics of anesthetic drugs in transgenic LQT1 and LQT2 rabbits reveal genotype-specific differential effects on cardiac repolarization. Am J Physiol Heart Circ Physiol 2008;295:H2264-72.

[44] Hansen DE. Mechanoelectrical feedback effects of altering preload, afterload, and ventricular shortening. Am J Physiol 1993;264:H423-32.

[45] Zeng J, Rudy Y. Early afterdepolarizations in cardiac myocytes: mechanism and rate dependence. Biophys J 1995;68:949-64.

[46] Chang MG, Chang CY, de Lange E, Xu L, O'Rourke B, Karagueuzian HS, Tung L, Marbán E, Garfinkel A, Weiss JN, Qu Z, Abraham MR. Dynamics of early afterdepolarization-mediated triggered activity in cardiac monolayers. Biophys J 2012;102:2706-14.

[47] Rizas KD, Nieminen T, Barthel P, Zürn CS, Kähönen M, Viik J, Lehtimäki T, Nikus K, Eick C, Greiner TO, Wendel HP, Seizer P, Schreieck J, Gawaz M, Schmidt G, Bauer A. Sympathetic activity-associated periodic repolarization dynamics predict mortality following myocardial infarction. J Clin Invest 2014;124:1770-80.

[48] Malliani A, Pagani M, Lombardi F, Cerutti S. Cardiovascular neural regulation explored in the frequency domain. Circulation 1991;84:482-92. Review.

[49] Furlan R, Porta A, Costa F, Tank J, Baker L, Schiavi R, Robertson D, Malliani A, Mosqueda-Garcia R. Oscillatory patterns in sympathetic neural discharge and cardiovascular variables during orthostatic stimulus. Circulation 2000;101:886-92.

[50] Child N, Hanson B, Bishop M, Rinaldi CA, Bostock J, Western D, Cooklin M, O'Neil M, Wright M, Razavi R, Gill J, Taggart P. Effect of mental challenge induced by movie clips on action potential duration in normal human subjects independent of heart rate. Circ Arrhythm Electrophysiol 2014;7:518-23.

[51] Koumi S, Backer CL, Arentzen CE, Sato R. beta-Adrenergic modulation of the inwardly rectifying potassium channel in isolated human ventricular myocytes. Alteration in channel response to beta-adrenergic stimulation in failing human hearts. J Clin Invest 1995;96:2870-81.

[52] Szentandrássy N, Farkas V, Bárándi L, Hegyi B, Ruzsnavszky F, Horváth B, Bányász T, Magyar J, Márton I, Nánási PP. Role of action potential configuration and the contribution of Ca^{2+} and K^+ currents to isoprenaline-induced changes in canine ventricular cells. Br J Pharmacol 2012;167:599-611.

[53] Ruzsnavszky F, Hegyi B, Kistamás K, Váczi K, Horváth B, Szentandrássy N, Bányász T, Nánási PP, Magyar J. Asynchronous activation of calcium and potassium currents by isoproterenol in canine ventricular myocytes. Naunyn Schmiedebergs Arch Pharmacol 2014;387:457-67.

[54] Zabel M, Koller RS, Sachs F, Franz MR. Stretch-induced voltage changes in the isolated beating heart: importance of the timing of stretch and implications for stretch-activated channels. Cardiovasc Res 1996;32:120-30.

[55] Kuijpers HL, Hermeling E, Lumens J, ten Eikelder HMM, Delhaas T, Prinzen FW. Mechano-electrical coupling as a framework for understanding functional remodeling during LBBB and CRT. Am J Physiol Heart Circ Physiol 2014;306:H1644-59.

[56] ter Keurs HE. The interaction of Ca2+ with sarcomeric proteins: role in function and dysfunction of the heart. Am J Physiol Heart Circ Physiol 2012;302:H38-50.

[57] Calaghan SC, Belus A, White E. Do stretch-induced changes in intracellular calcium modify the electrical activity of cardiac muscle? Prog Biophys Mol Biol 2003;82:81-95.

[58] Weiss JN, Garfinkel A, Karagueuzian HS, Ngugen TP, Olcese R, Chen PS, Qu Z. Perspective: a dynamics-based classification of ventricular arrhythmias. J Mol Cell Cardiol 2015;82:136-52.

[59] Oosterhoff P, Tereshchenko LG, van der Heyden MA, Ghanem RN, Fetics BJ, Berger RD, Vos MA. Short-term variability of repolarization predicts ventricular tachycardia and sudden cardiac death in patients with structural heart disease: a comparison with QT variability index. Heart Rhythm 2011;8:1584-90.

[60] Tereshchenko LG, Fetics BJ, Domitrovich PP, Lindsay BD, Berger RD. Prediction of ventricular tachyarrhythmias by intracardiac repolarizationvariability analysis. Circ Arrhythm Electrophysiol 2009;2:276-84.

[61] Atiga WL, Calkins H, Lawrence JH, Tomaselli GF, Smith JM, Berger RD. Beat-to-beat repolarization lability identifies patients at risk for sudden cardiac death. J Cardiovasc Electrophysiol 1998;9:899-908.

[62] Grandi E, Pasqualini FS, Pes C, Corsi C, Zaza A, Severi S. Theoretical investigation of action potential duration dependence on extracellular Ca2+ in human cardiomyocytes. J Mol Cell Cardiol 2009;46:332-42.

[63] Verrier RL, Antzelevitch C. Autonomic aspects of arrhythmogenesis: the enduring and the new. Curr Opin Cardiol 2004;19:2-11.

[64] Rubart M, Zipes DP. Mechanisms of sudden cardiac death. J Clin Invest 2005;115:2305-15.

[65] Rosenbaum DS, Jackson LE, Smith JM, Garan H, Ruskin JN, Cohen RJ. Electrical alternans and vulnerability to ventricular arrhythmias. N Engl J Med 1994;330:235-41.

[66] Coote JH. Multiple oscillators in autonomic control. J Physiol 2001;533:2.

[67] Gilbey MP. Multiple oscillators, dynamic synchronization and sympathetic control. Clinical and Exper Pharmacol Physiol 2001;28:130-7.

[68] Malpas SC. Neural influences on cardiovascular variability: possibilities and pitfalls. Am J Physiol Heart Circ Physiol 2002;282:H6-20.

[69] Morris KF, Nuding SC, Segers LS, Baekey DM, Shannon R, Lindsey BG, Dick TE. Respiratory and Mayer wave-related discharge patterns of raphe and pontine neurons change with vagotomy. J Appl Physiol 2010;109:189-202.

[70] Zhou S, Jung BC, Tan AY, Trang VQ, Gholmieh G, Han SW, Lin SF, Fishbein MC, Chen PS, Chen LS. Spontaneous stellate ganglion nerve activity and ventricular arrhythmia in a canine model of sudden death. Heart Rhythm 2008;5:131-9.

[71] Johnson DM, Heijman J, Bode EF, Greensmith DJ, van der Linde H, Abi-Gerges N, Eisner DA, Trafford AW, Volders PG. Diastolic spontaneous calcium

release from the sarcoplasmic reticulum increases beat-to-beat variability of repolarization in canine ventricular myocytes after β-adrenergic stimulation. Circ Res 2013;112:246-56.

[72] Heijman J, Zaza A, Johnson DM, Rudy Y, Peeters RL, Volders PG, Westra RL. Determinants of beat-to-beat variability of repolarization duration in the canine ventricular myocyte: A computational analysis. PLoS Comput Biol 2013;9:e1003202.

[73] Chang HS, Staras K, Gilbey MP. Multiple oscillators provide metastability in rhythm generation. J Neurosci 2000;20:5135-43.

[74] Myles RC, Wang L, Kang CI, Bers DM, Ripplinger CM. Local β-adrenergic stimulation overcomes source-sink mismatch to generate focal arrhythmia. Circ Res 2012;110:1454-64.
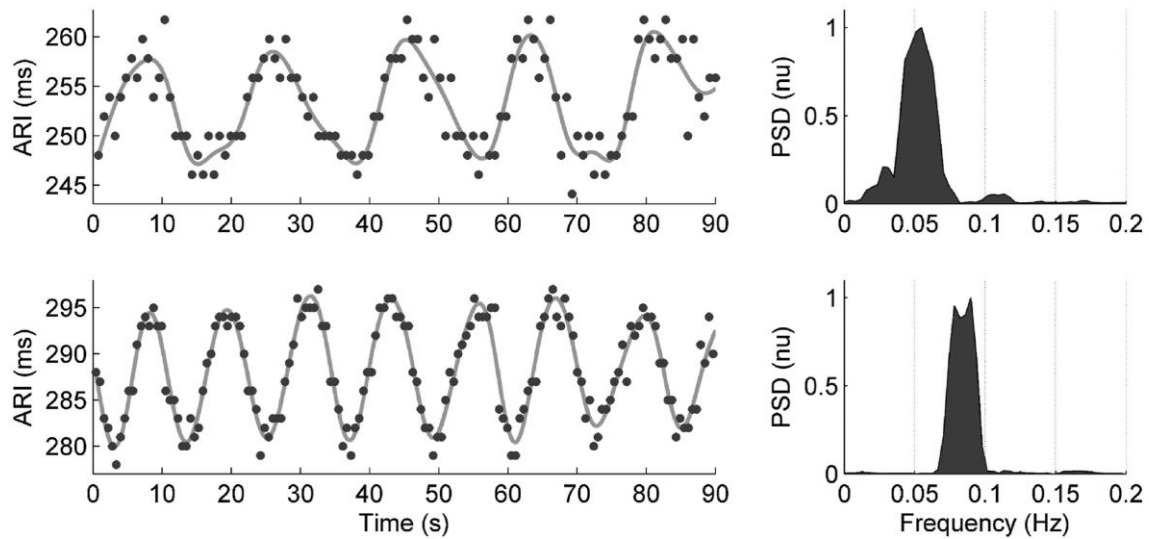
Figure 1. Activation recovery interval (ARI), a standard surrogate for APD, oscillating at a frequency of 0.06 Hz (top), i.e. 18-second period, and 0.08 Hz (bottom), i.e. 13-second period. Circles represent beat-to-beat ARIs, while solid lines represent low-frequency trends. Power spectral densities (PSD) of ARI series are shown on the right hand side.
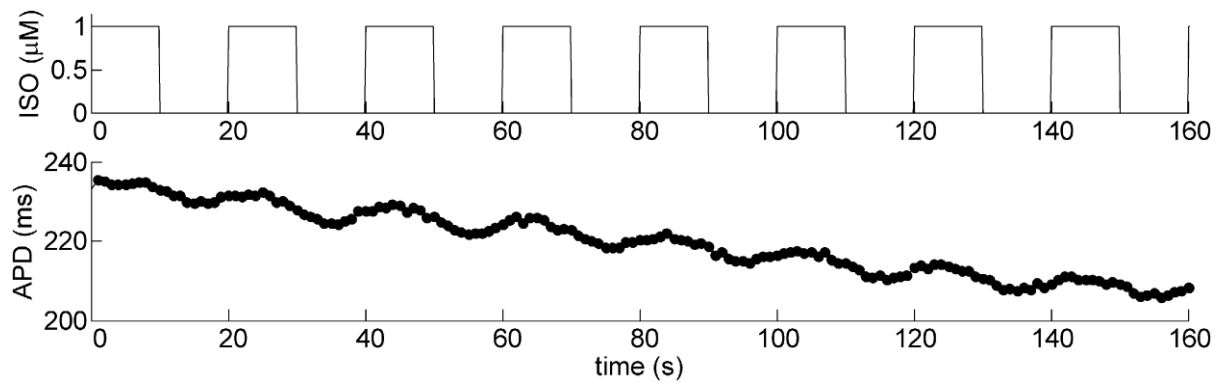

Figure 2. Protocol of phasic isoproterenol (ISO) application (top panel) and corresponding time course of action potential duration (APD) changes (bottom panel) computed using the O'Hara-Xie-modNiederer model.
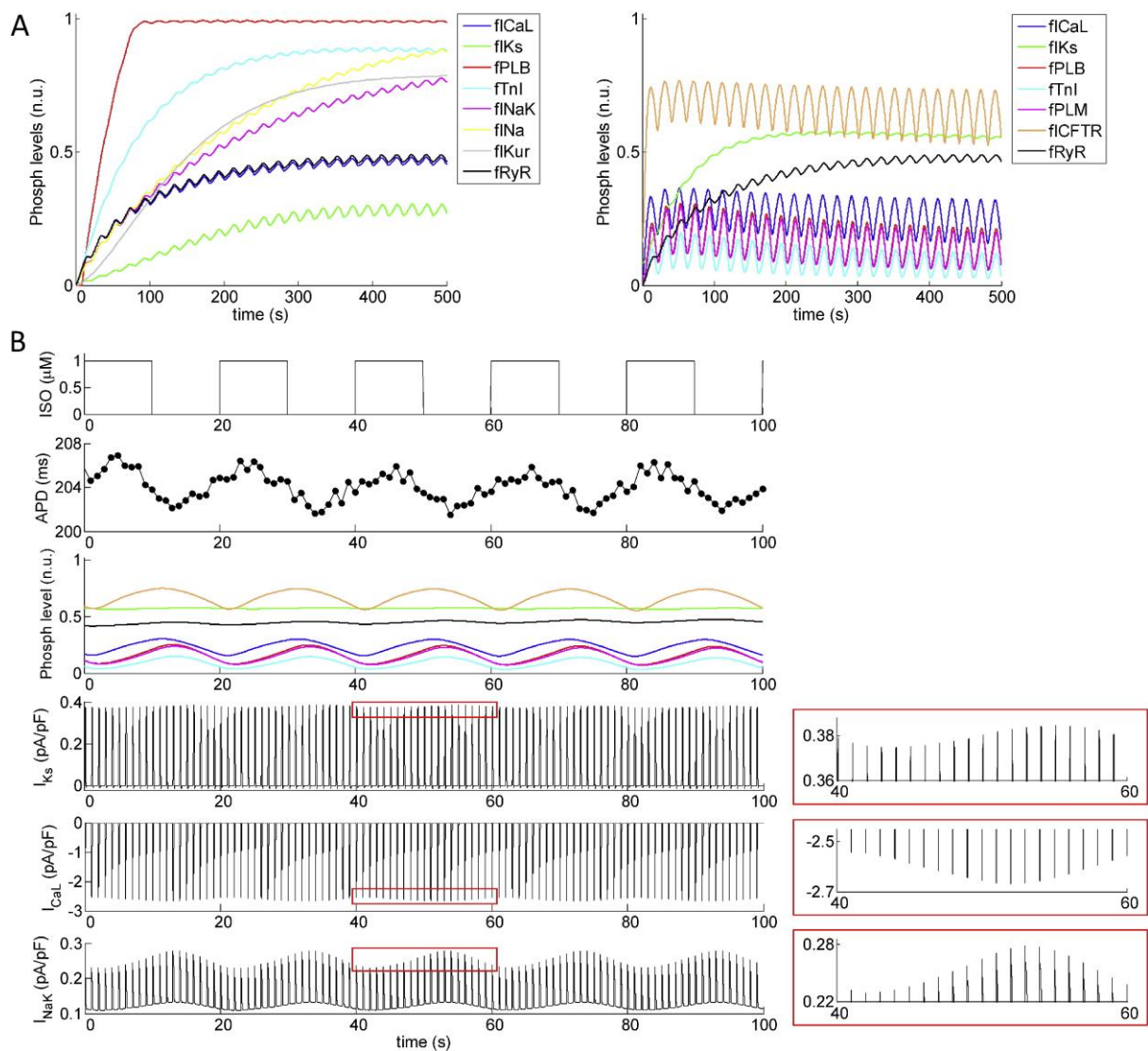
Figure 3. A) Phosphorylation (Phosph) levels of PKA substrates elicited during a 500-second protocol of isoproterenol (ISO) application like that shown in Figure 2, computed using the Heijman (left panel) and Xie (right panel) formulations described in section 2.3. In the left panel, fICaL, fIKs, fPLB, fTnI, fINaK, fINa, fIKur and fRyR denote the fractions of phosphorylated L-type calcium (ICaL), slowed delayed rectifier potassium (IKs), phospholamban (PLB), inhibitory troponin subunit (TnI), Na$^+$/K$^+$ pump (INaK), sodium (INa), ultrarapid plateau potassium (IKur) and ryanodine receptor (RyR) computed with the Heijman formulation. In the right panel, similarly for the Xie model, with fPLM and fICFTR denoting the fraction of phosphorylated phospholemman (PLM) and cystic fibrosis transmembrane regulator (ICFTR). B) Action potential duration (APD) oscillations at a frequency of 0.05 Hz (second row) following a period of prolonged phasic beta-adrenergic stimulation (first row), phosphorylation (phosph) levels of PKA substrates (third row) and time course of three currents (I$_{Ks}$, I$_{CaL}$ and I$_{NaK}$, last three rows) with major effects on the APD response to β-AS, as computed with the O'Hara-Xie-modNiederer model. In Figure 3B, 0 in the x axis represents 270 s following phasic β-AS.
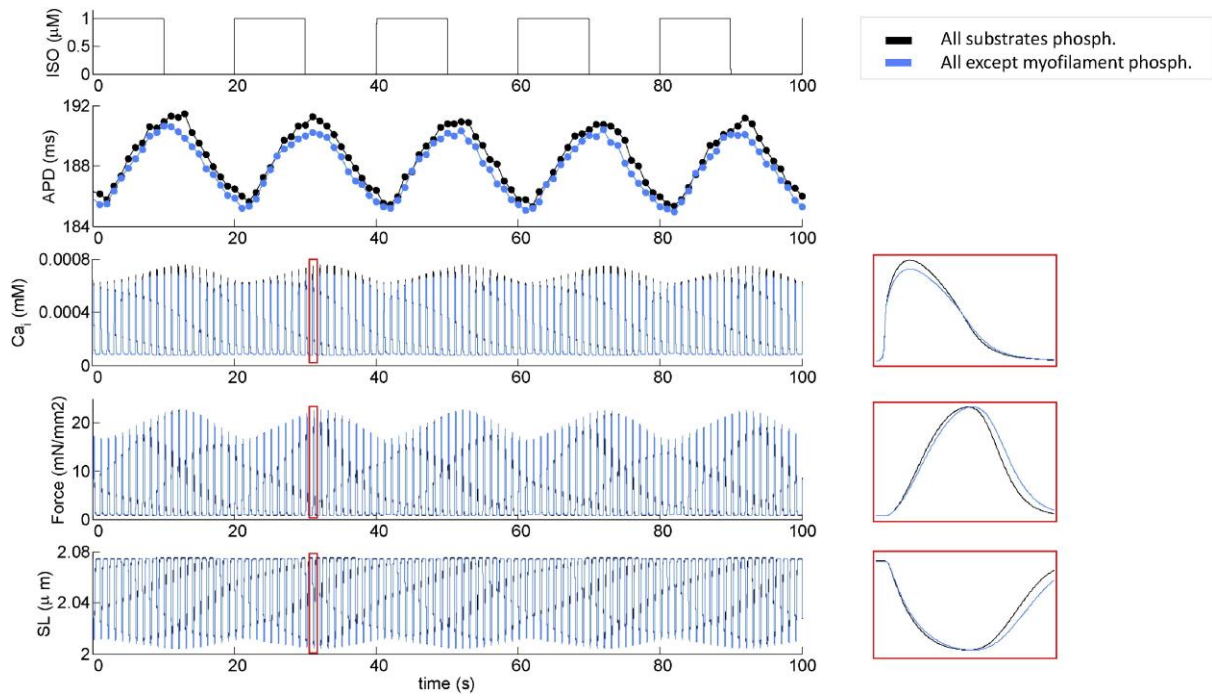
Figure 4. Effects of prolonged phasic β-AS (first row, isoproterenol concentration (ISO)) on action potential duration (APD) oscillations at 0.05 Hz (second row) with PKA phosphorylation of all substrates (black) and with myofilament phosphorylation disabled (blue) in the Negroni model. In rows 3 to 5 corresponding time courses of free Ca^{2+} concentration (Ca_i), isometric force and sarcomere length (SL) are shown. 0 in the x axis represents 270 s following phasic β-AS.
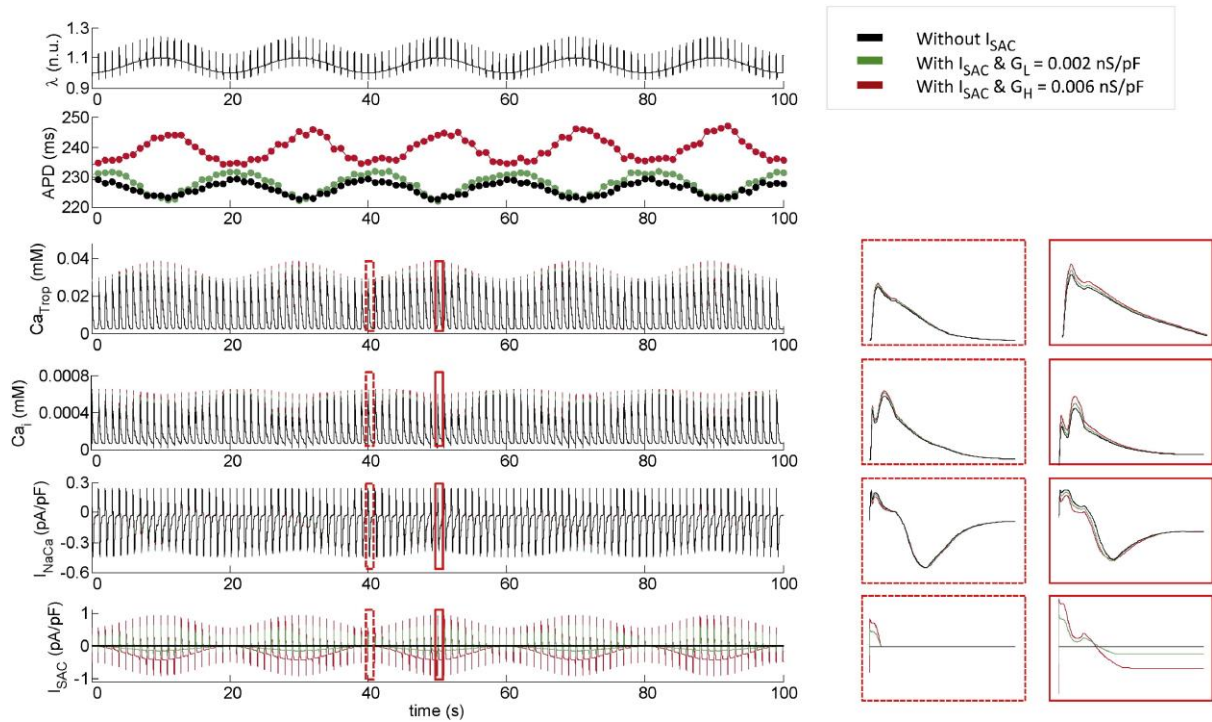
Figure 5. Effects of prolonged phasic stretch of up to 10% (first row, stretch ratio (λ)) on action potential duration (APD) oscillations at 0.05 Hz (second row) in the absence (black, G_0) and presence of stretch-activated channels (SACs) with low (green, G_L) and high (red, G_H) $G_{SAC,ns}$ (see section 2.4). Rows 3 to 5 illustrate how stretch increases the amount of Ca^{2+} bound to troponin (Ca_{Trop}), decreases the amplitude of free cytosolic Ca^{2+} (Ca_i) and causes a reduction in the inward Na^+-Ca^{2+} exchanger current (I_{NaCa}) of the O'Hara-Xie-modNiederer model. These stretch-induced changes, together with the contribution of SACs (sixth row, current through stretch-activated channels (I_{SAC})), modulate APD and lead to the observed cyclic changes. 0 in the x axis represents 270 s following phasic stretch.
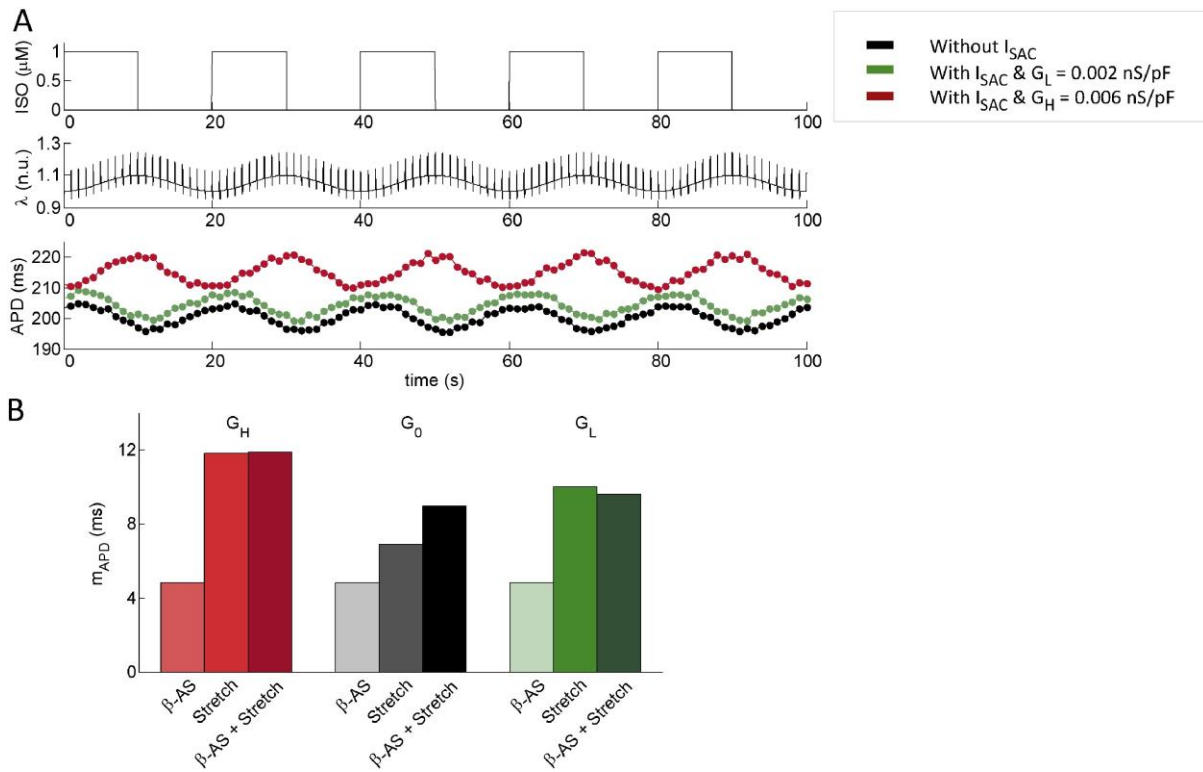
Figure 6. A) Effects of combined prolonged phasic β-AS (top panel, isoproterenol concentration (ISO)) and stretch (middle panel, stretch ratio (λ)) on action potential duration (APD) oscillations at 0.05 Hz (bottom panel) for the same three cases illustrated in Figure 5 corresponding to absence (black, G_0) and presence of stretch-activated channels (SACs) with low (green, G_L) and high (red, G_H) $G_{SAC,ns}$. 0 in the x axis represents 270 s following phasic β-AS and stretch. B) Summary of the corresponding maximal magnitude of APD oscillations (m_{APD}) following prolonged phasic β-AS only, phasic stretch only and combined phasic β-AS and stretch in the O'Hara-Xie-modNiederer model.
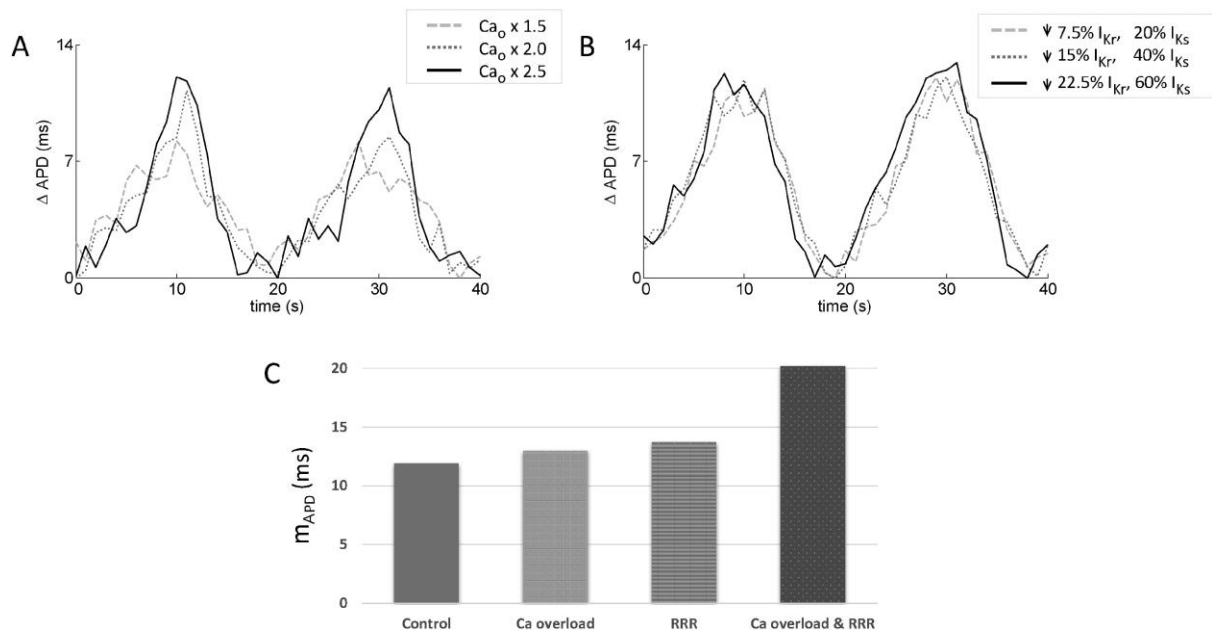
Figure 7. A) Magnitude of action potential duration (APD) oscillations (Δ APD) at 0.05 Hz following prolonged combined phasic β-AS and stretch under Ca^{2+} overload conditions simulated by increasing extracellular Ca^{2+} concentration (Ca_o) by factors of 1.5 (dashed light grey), 2.0 (dotted dark grey) and 2.5 (solid black). B) Magnitude of APD oscillations (Δ APD) at 0.05 Hz under reduced repolarization reserve (RRR) conditions simulated by inhibiting the rapid and slowed delayed rectifier potassium currents, I_{Kr} and I_{Ks}, by 7.5% and 20% (dashed light grey), 15% and 40% (dotted dark grey) and 22.5% and 60% (solid black). C) Summary of maximal magnitude of APD oscillations (m_{APD}) for control, Ca^{2+} overload (Figure 7A), RRR (Figure 7B) and combined Ca^{2+} overload and RRR conditions. In all cases the O'Hara-Xie-modNiederer model with high $G_{SAC,ns}$ was used. 0 in the x axis represents 270 s following phasic β-AS and stretch.
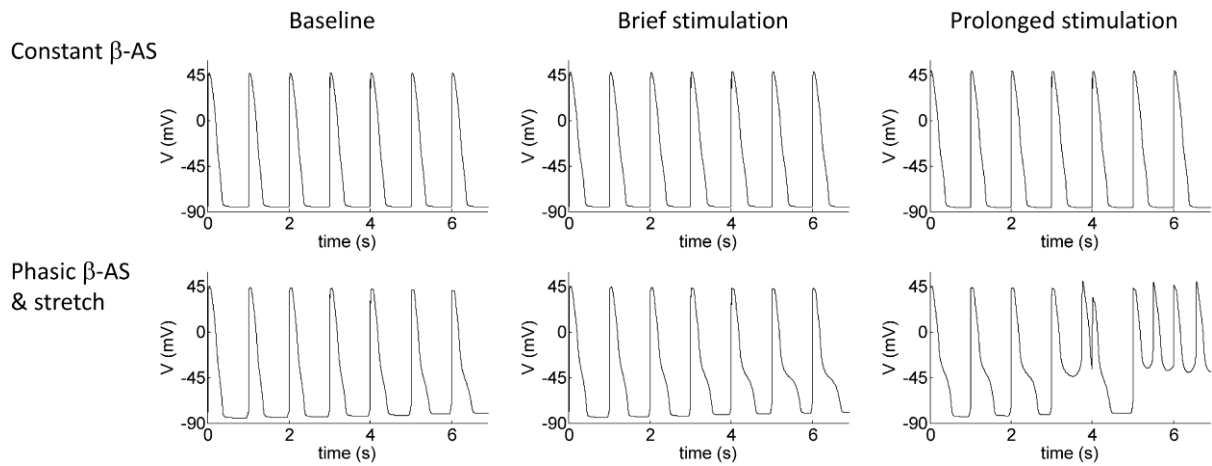
Figure 8. Time course of transmembrane potential (V) at baseline (left column) and following brief (middle column) and prolonged (right column) periods of β-AS. Baseline corresponds to simulation of Ca^{2+} overload (4-fold increase in extracellular Ca^{2+}) and RRR (30% I_{Kr} and 80% I_{Ks} inhibition). Constant β-AS with 1 μM ISO (first row) only slightly modifies the AP morphology, while phasic β-AS and stretch (second row) severely alter the AP leading to arrhythmogenic events. In these simulations the O'Hara-Xie-modNiederer model was used, with $G_{SAC,ns}$ = 0.01 nS/pF.

INVESTIGATED EFFECT	MODEL NAME	ELECTROPHYSIOLOGY	PKA	MECHANICS	JUSTIFICATION FOR USE
β-AS effects (sections 3.1 & 3.2)	O'Hara - Xie- modNiederer	O'Hara	Xie	modNiederer (stretch not tested)	Default model (justified in text)
	O'Hara - Heijman - modNiederer	O'Hara	Heijman	modNiederer (stretch not tested)	Assess β-AS effects with a different PKA formulation
	Decker - Heijman	Decker	Heijman		Assess β-AS effects on a dog-specific model
	Shannon - Soltis	Shannon	Soltis (with updates)		Assess β-AS effects on a rabbit-specific model
	Negroni	Shannon	Soltis (with updates)	Negroni (stretch only as induced by β-AS)	Assess β-AS effects on electrical and mechanical targets
Stretch effects (section 3.3)	O'Hara - modNiederer	O'Hara		modNiederer	Default model (justified in text)
	ten Tusscher - modNiederer	ten Tusscher		modNiederer	Assess stretch effects on a different electrophysiological model
	ten Tusscher - Rice	ten Tusscher		Rice	Assess stretch effects on a different mechanical model that includes SL variations within each cycle
	ten Tusscher - Niederer	ten Tusscher		Niederer (human characteristics)	Assess stretch effects on a mechanical model that does not include SL variations within cycle
	O'Hara - Niederer	O'Hara		Niederer (human characteristics)	Assess stretch effects on a mechanical model that does not include SL variations within cycle

	Terkildsen	Pandit-Hinch		Niederer (original, rat characteristics)	Assess stretch effects on a rat-specific model
β-AS & stretch effects (section 3.4)	O'Hara - Xie-modNiederer	O'Hara	Xie	modNiederer	Default model (justified in text)
	O'Hara - Xie-Niederer	O'Hara	Xie	Niederer	Assess β-AS & stretch effects with a mechanical model that does not include SL variations within cycle
Disease conditions (section 3.5)	O'Hara - Xie-modNiederer	O'Hara	Xie	modNiederer	Default model (justified in text)
	O'Hara - Heijman - modNiederer	O'Hara	Heijman	modNiederer	Assess arrhythmogenic behavior with a different PKA formulation
	Negroni	Shannon	Soltis (with updates)	Negroni	Assess arrhythmogenic behavior with a model that includes β-AS effects on electrical and mechanical targets

Table 1. Combined electrophysiological, PKA and mechanical models used in this study. The first column indicates the effects investigated with the models and the sections containing the corresponding results in the text. The second column contains the name of the combined model as used in the text. The third, fourth and fifth column describe the individual electrophysiological, PKA and mechanical formulations assembled in the combined model. The sixth column justifies the reason for introducing each of the models in the study.